Neutron spin structure from e-³He scattering with double spectator tagging at the electron-ion collider

I. Friščić [a,b,1,2], D. Nguyen [a,b,1], J.R. Pybus [a,b], A. Jentsch [c], E.P. Segarra [a], M.D. Baker [d], O. Hen [a], D.W. Higinbotham [b,*], R. Milner [a], A.S. Tadepalli [b], Z. Tu [c], J. Rittenhouse West [b,e]

[a] *Laboratory for Nuclear Science, Massachusetts Institute of Technology, Cambridge, MA 02139, USA*
[b] *Thomas Jefferson National Accelerator Facility, Newport News, VA 23606, USA*
[c] *Department of Physics, Brookhaven National Laboratory, Upton, NY 11973, USA*
[d] *Mark D. Baker Physics and Detector Simulations LLC, Miller Place, NY 11764, USA*
[e] *Nuclear Science Division, Lawrence Berkeley National Laboratory, Berkeley, CA 94720, USA*

A R T I C L E   I N F O

A B S T R A C T

The spin structure function of the neutron is traditionally determined by measuring the spin asymmetry of inclusive electron deep inelastic scattering (DIS) off polarized ³He nuclei. In such experiments, nuclear corrections are significant and must be treated carefully in the interpretation of experimental data. Here we study the feasibility of suppressing model dependencies by tagging both spectator protons in the process of DIS off neutrons in ³He at the forthcoming Electron-Ion Collider (EIC). This allows for a reconstruction of the momentum of the struck neutron to ensure it was nearly at rest in the initial state, thereby reducing sensitivity to nuclear corrections and suppressing contributions from electron DIS off protons in ³He. Using realistic accelerator and detector configurations, we demonstrate that the EIC can probe the neutron spin structure from x_B of 0.003 to 0.651. We find that the double spectator tagging method results in reduced uncertainties by a factor of 2 on the extracted neutron spin asymmetries over all kinematics and by a factor of 10 in the low-x_B region, thereby providing valuable insight into the spin and flavor structure of nucleons.

1. Introduction

The decomposition of nucleon spin in terms of quark spin, quark orbital angular momentum and total gluon angular momentum is a fundamental challenge in hadronic physics [1,2]. Experiments have found that quarks carry only around 30% of the total spin of the nucleon [3,4] and future experiments are aimed at pinning down the contribution of the Orbital Angular Momentum (OAM) of the quarks in the valence region and gluon angular momentum [5]. Previous results hint at quark OAM contributions to the neutron spin [6]. Precise data is essential to test nucleon spin theories, in particular for the valence quark spin contributions where the contributions to spin from sea quark and anti-quark pairs as well as gluons are expected to be small [7,8].

While stable particles such as hydrogen are readily available for studies of the proton structure, it is extremely challenging to make

even low luminosity neutron beams [9]. Instead, physicists have made use of deuterium and ³He targets as effective neutron targets in order to extract unpolarized nucleon structure functions F_1 and F_2 [10,11], polarized spin structure functions g_1 and g_2 [12,13], as well as virtual photon asymmetry A_1 [14]. Of partiulcar interest, A_1 is defined as $A_1 = (\sigma_{1/2} - \sigma_{3/2})/(\sigma_{1/2} + \sigma_{3/2})$ where subscript $1/2(3/2)$ is the projection of the total spin along the direction of the virtual photon momentum. Although polarized deuterium would allow for a single proton spectator tagged final state, it is not planned in the initial phase of Electron-Ion Collider (EIC) operations due to technical challenges related to the gyromagnetic ratio of the deuteron as compared to protons ($\gamma_D/\gamma_p = 0.047$) and ³He ($\gamma_D/\gamma_{³He} = 0.081$) [15]. On other hand, work is already underway on developing a polarized ³He sources for the EIC [16] and it is within the scope of the initial project that polarized ³He beams will be able to be stored.
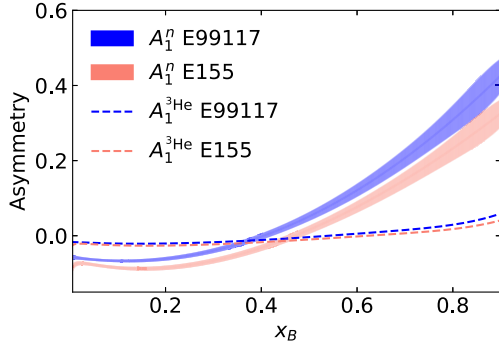
A novel experimental method for minimizing corrections due to off-shell neutron effects as well as deep inelastic scattering events from protons in ³He is to tag the recoiling spectator proton(s) from the target. This was done recently in the Jefferson Lab BONuS experiment [17,18] with deuterium in which neutron deep inelastic

---

Fig. 1. The asymmetries A_1^n (bands) and $A_1^{3\text{He}}$ (dashed-line) as a function of x_B at $Q^2 = 5$ (GeV/c)^2. The two $A_1^{3\text{He}}$ curves were calculated using A_1^p parameters in [14] and A_1^n parameters in [14] [E99117] and [27] [E155] following a simple estimation based on formula (3). The bands show the extracted A_1^n from $A_1^{3\text{He}}$ as described in section 8.

Fig. 2. A diagram of Deep Inelastic $e+^3$He scattering with double spectator tagging. The channel shown here is electron scattering off a neutron in ^{3}He; the two spectator nucleons are the protons in the process ^{3}He($e, e' p_{s1} p_{s2}$)X.

Fig. 3. Zoomed-in image of a 3BBU-MF $e+^3$He with both protons tagged in the Roman Pot silicon detector planes. The beam pipe was made semi-transparent in order to see the event. The off-momentum detectors are omitted from the figure to make the event easier to view.

scattering events were selected by requiring the detection of an accompanying low momentum proton. By ensuring the recoiling momentum of the proton is small, the experiment maximizes the probability that the electron has undergone deep inelastic scattering on a nearly free neutron [19]. This technique minimizes the model dependence of the extraction of the neutron information and avoids many of the theoretical problems involved with extracting neutron information from inclusive scattering from a nuclear target [20,21].

Unfortunately, this same technique has never been done with fixed target polarized ^{3}He targets, where the low momentum recoil protons would need to pass through the glass of the target cell walls in order to be detected. Thus, to date, the neutron structure functions are extracted from ^{3}He measurements and require large model dependent corrections from the measured cross sections and asymmetries to extract the quantities of interest [13,22]. In Fig. 1 we show the large difference between the measured quantities and the extracted neutron information.
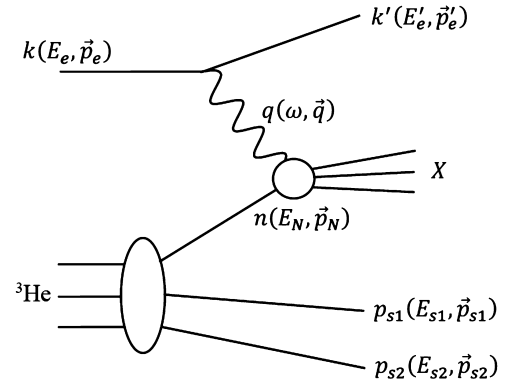
While our knowledge of the three-body system and nuclear corrections is good, it is clearly not perfect as has been shown experimentally [23–26]. Traditionally, one measures the DIS off the polarized ^{3}He to determine the virtual photon asymmetry $A_1^{3\text{He}}$, and then deduces the neutron asymmetry A_1^n. In this procedure the model dependent proton polarization used as an input in extraction dominates the total systematic uncertainty [14]. Therefore, while accurate measurements of A_1^p exist for the proton, more precise data on effective polarized neutron targets are necessary.

With high energy electron and ^{3}He beams at the EIC, it is possible to detect recoiling spectator protons with low momentum in the rest frame of ^{3}He. These recoil protons, which have a high momentum in the lab frame, can be detected in the far forward region of the EIC. This unique tagging capability will ensure that the electron interacted with a nearly free initial-state neutron and allows an extraction of neutron spin structure with less model-dependence and more precision than inclusive techniques.
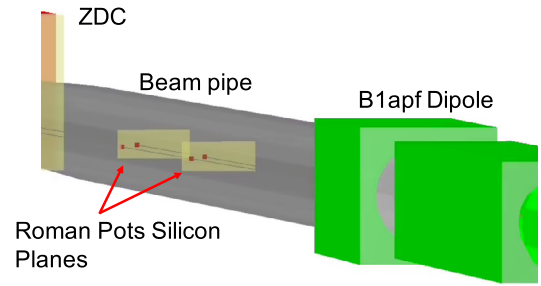
2. DIS kinematics with double spectator tagging

High energy electron beams have made it possible to access DIS kinematics. This region corresponds to scattering well beyond the nucleon resonances [28] and is experimentally accessed by going to large four-momentum squared transfer $Q^2 \equiv -q^2 \geq 2$ (GeV/c)^2 and large hadronic system invariant mass $W^2 \geq 4$ (GeV/c)^2.

A DIS electron-nucleon event is defined by the initial four-momentum of the electron and nucleon $k = (E_e, \vec{k}_e)$, $p = (E_p, \vec{p})$, respectively, the final four-momentum of the electron $k' = (E'_e, \vec{k}'_e)$ and the four-momentum transfer $q = k - k'$. In the case of electron-

nucleus scattering, p defines the four-momentum of an on-mass-shell nucleon at rest within the nucleus. We define the following quantities for the event:

- the Bjorken variable $x_B = \frac{Q^2}{2(q \cdot p)}$, where $Q^2 = -q^2$ is minus the four-momentum transfer squared;
- the fractional energy transfer $y = \frac{q \cdot p}{k \cdot p}$;
- the final hadronic system squared invariant mass $W^2 = (q + p)^2$;
- the energy of the beam electron E_e;
- the energy E'_e, opening angle θ'_e, and azimuthal angle ϕ'_e of the scattered electron.

For the nuclear system, we define the initial four-momentum of the nucleus p_A and the initial four-momentum of the nucleons p_i. Here $i = 1, s1, s2$, where nucleon 1 is the struck nucleon and nucleons $s1$ and $s2$ are the spectator nucleons, as shown in Fig. 2. For each nucleon we also define, in the nuclear rest frame:

- the momentum perpendicular to the momentum transfer $\mathbf{p}_i^\perp$;
- the "plus/minus" component of momentum $p_i^\pm = E_i \pm p_i^z$, where the z-component is defined parallel to the momentum transfer;
- the light-front momentum fraction $\alpha_i = \frac{A}{m_A} p_i^-$ where A is the atomic mass number and m_A is the target mass.

Finally, we define the virtuality of the struck nucleon $v = m_N^2 - (p_A - p_{s1} - p_{s2})^2$.

Table 1

The relative strength of breakup regimes.

Regime	Proton fraction	Neutron fraction
2BBU	67%	–
3BBU-MF	27%	90%
SRC	6%	10%

3. Event generator and Fermi motion correction

DIS events were generated using the CLASDIS generator, a CLAS version of PEPSI [29] generator, which is based on LEPTO version 6.5 and JETSET version 7.410. The generator is also capable of generating semi-inclusive DIS (SIDIS) events. The CLASDIS generator is intended to be used for the fixed target event generation (electron beam goes along $+z$ direction); in order to use it for the EIC kinematics (ion beam goes along $+z$ direction and the electron beam goes into opposite direction), the selected EIC kinematics in terms of electron and ion beam energies need to be boosted in the fixed target frame, in which the ion beam is at rest and the energy of the electron beam is Lorentz-boosted. Events are then generated in the fixed target frame using the CLASDIS generator and boosted back into the collider frame of the EIC.

CLASDIS can generate (SI)DIS events for polarized and unpolarized targets, but is currently only capable of generating DIS events from free protons and free neutrons. CLASDIS approximates ^{3}He electron scattering events by combining the scattering from three free nucleons (two protons, one neutron). This approximation does not include the effects of the Fermi motion of the nucleons inside the nucleus on generated DIS events, nor are the kinematics of the spectators (nucleons or nuclei) considered. A separate procedure was therefore developed to account for each of these effects.

Nuclear corrections to DIS were modeled within three breakup regimes depending on the momentum of the struck nucleon and the excitation of the residual system. The three breakup regimes were classified as 2-body breakup (2BBU), mean-field 3-body breakup (3BBU-MF), and short-range correlation breakup (SRC).

In the 2BBU regime momentum of the leading nucleon is given by the Ciofi-Kaptari spectral function [30], which constrains the momentum of the residual nucleus. For the 3BBU-MF regime, the momentum of the leading nucleon and the energy of the spectator system were taken from the Ciofi-Kaptari spectral function [30], which is truncated at a leading nucleon momentum of 240 MeV/c to provide separation from the SRC-dominated regime and ensure the predicted SRC pair fractions. The magnitude of the relative momentum of the spectator system was determined from the system's energy, and the direction was sampled assuming an isotropic distribution. In the case of the SRC regime, the relative momentum and center-of-mass momentum of the leading pair were determined using the light-front Generated Contact Formalism (GCF) [31], which constrained the momentum of the residual nucleon.

The relative strengths of the 2BBU regime [30] and SRC regime [32] were used to constrain the population of the 3BBU-MF regime, as listed in Table 1.

In order to add nuclear effects to each CLASDIS generated events, calculations were conducted on the light-front, meaning that the light-front fraction and transverse momentum for each nucleon was required, rather than the standard 3-momentum. The GFC calculations already included this [31], but for the Ciofi-Kaptari spectral function it was necessary to move the initially sampled kinematics to the light-front. The Frankfurt-Strikman formalism [33], developed for the deuteron on the light-front, was generalized as follows: for each particle, the momentum was determined, and the energy was selected to place the particle on-shell, resulting in temporary violation of energy conservation ($\sum_i E_i \neq m_A$). The system was then Lorentz boosted into a

Table 2

Summary of basic polar scattering angle acceptance and average p_T smearing for each FF detector subsystem. Details can be found in the EIC Yellow Report [35].

Detectors	θ Acc. [mrad]	p_T res. [MeV/c]
B0 tracker	[5.5, 20.0]	15–30
Off-momentum	[0.0, 5.0]	20–30
Roman Pots	[0.0, 5.0]	20–30
ZDC	[0.0, 4.5]	30–40

frame where the minus momentum ($p^- \equiv E - p_z$) was conserved ($\sum_i p_i^- = m_A$), leaving the plus momentum ($p^+ \equiv E + p_z$) unconserved ($\sum_i p_i^+ \neq m_A$). This provided satisfaction of the light-front baryon and momentum sum rules [33]. The effects of this boost were relatively small, resulting in nonconservation of the plus momentum on the order of 30 MeV/c. Light-front effects were more significant in the high-momentum SRC regime, where the GCF calculations were performed manifestly on the light-front.

Events taken from the CLASDIS generator were adjusted to account for nuclear motion. Considering only inclusive scattering, the free-nucleon events are described by a cross section

$$\frac{d^3\sigma}{dx_B dy d\phi_e'} \equiv \sigma_{free}(x_B, y, \phi_e') \tag{1}$$

described in [29]. By altering the kinematics to replace the Bjorken scaling variable x_B with the scaling variable $x' = x_B/\alpha_1$ which includes the smearing effects of nuclear motion, we change the effective cross section to one which performs a convolution between the free DIS cross section and the light-front nuclear spectral function:

$$\frac{d^9\sigma}{dx'dyd\phi_e'\frac{d\alpha_{s1}d^2\mathbf{p_{s1}^\perp}}{\alpha_{s1}}\frac{d\alpha_{s2}d^2\mathbf{p_{s2}^\perp}}{\alpha_{s2}}} = \sigma_{free}(x', y, \phi_e')S(\alpha_{s1}, \mathbf{p_{s1}}, \alpha_{s2}, \mathbf{p_{s2}})$$

where $S(\alpha_{s1}, \mathbf{p_{s1}}, \alpha_{s2}, \mathbf{p_{s2}})$ is the light-front spectral function describing the structure of the nucleus, including all regimes previously described. After sampling the spectral function, modifying the CLASDIS events to account for the nuclear motion, and adding the spectator protons, we receive a sample of tagged DIS events described by the above cross section.

4. Full detector simulations with EicRoot

Realistic detector simulations have been carried out using the EIC reference detector far-forward (FF) configuration implemented in the EicRoot simulation framework, which makes use of the ROOT Virtual Monte Carlo structure and GEANT4 [34].

The FF detector subsystems, shown in Fig. 3, are optimized to try and cover as much of the acceptance at $\eta > 4.5$ as possible. Table 2 summarizes the geometric acceptances and ranges of typical absolute transverse momentum smearing for the four FF detector subsystems, each of them covering different regions of the FF acceptance and a unique area of the phase space.

The first detector along the hadron beamline after the interaction point is the B0 detector, which is comprised of silicon tracking layers inside the B0pf dipole magnet. This subsystem is used for capturing charged particles at larger scattering angles ($\theta > 5.5$ mrad).

The Roman Pots are situated ~ 27 meters downstream from the interaction point. They consist of silicon sensors placed in Roman Pot vessels or RF shields which are injected into the beam line vacuum a few mm from the hadron beam. The Roman Pots detector subsystem is used for capturing protons with smaller scattering angles ($\theta < 5$ mrad), but with a momentum similar to that of the

settings for the steering magnets, where the tagged proton momentum vs. beam magnet setting is referred to as the magnetic rigidity.

The Off-Momentum Detectors were designed to optimally tag charged particles with a rigidity $\sim \frac{1}{2}$ that of the beam, but otherwise have a similar acceptance and smearing contribution to that of the Roman Pots. They are placed outside the beam pipe in the same drift region as the Roman Pots detectors. This enables tagging of charged particles as they are bent out of the beam pipe by the last dipole magnet (B1apf) before the drift region.

The Zero-Degree Calorimeter (ZDC) will contain both hadronic and electromagnetic calorimetry and is used for tagging neutrons from nuclear breakup, as well as photons from coherent nuclear scattering.

Various effects impact the overall measured smearing in the momentum reconstruction. There are contributions from the detector assumptions which include the finite pixel size of the silicon detectors used in the B0 detector, Roman Pots detectors, and the Off-Momentum Detectors, as well as the assumptions used in the reconstruction (e.g. a linear transport matrix for the Roman Pots). There are also effects from the beam such as angular divergence and vertex smearing induced by the crab cavities used to compensate for the EIC crossing angle of 25 mrad. The details of the detector layout and assumptions can be found in the EIC Yellow Report [35], in a previous study of exclusive J/ψ production [36] and Conceptual Design Report [15].

5. Fast simulations with Eic-smear

Eic-smear is a Monte Carlo analysis package, which was developed by the BNL EIC task force. It is a collection of ROOT classes and routines for analysing Monte Carlo events and performing fast smearing to study the effects of detector resolution and it is optimized for processing of large amount of data. For our particular channel of interest the scattered electron is smeared with smearing functions for the central detector in the pseudo-rapidity range $-3.5 < \eta < 3.5$ and the two tagged protons in the far-forward region $\eta > 4.5$. The central detector consists of several different detector systems which cover their own range of pseudo-rapidity η and corresponding resolution of three-momentum p (tracking) and energy E (EM calorimeters). For tagged protons only the three-momentum p and transverse momentum P_t are smeared. The smearing is summarized in Table 3), which parameters correspond to the most updated version of the smearing matrix from November 21 2020 [37], as defined by the Yellow Report Detector working group.

6. Selected EIC kinematics

For the purpose of this paper, we have selected one of the two beam energies combinations from the Yellow Report [35]. The chosen electron beam energy was 5 GeV and ^{3}He beam had 41 GeV/nucleon (5x41). Since the CLASDIS generator assumes the fixed target kinematics, the electron beam was boosted into the frame in which the ^{3}He is at rest. In order to be in the DIS regime, events were generated with the following cuts: $Q^2 > 2$ (GeV/c)^2, $W^2 > 4$ (GeV/c)^2, $z > 0.2$ and $0.05 < y < 0.95$. Fermi corrections were applied to the generated events in the fixed target frame, which were then boosted into the collider frame. These events were then processed using the two different simulation frameworks EicRoot and Eic-smear. Fig. 4 shows the angular distribution of both tagged protons scattering angle θ_p, for each of the two relevant nuclear effects, 3BBU-MF and SRC, separately.

Table 3
Summary of relevant particle smearing configuration performed in Eic-smear software package, as defined in Matrix 02 [37], the newest (November 21 2020) detector matrix released by the EIC Yellow Report Detector working group.

η range	Tracking
-3.5 – -2.5	$\sigma_p/p \sim 0.2\% \cdot p + 5\%$
-2.5 – -1.0	$\sigma_p/p \sim 0.04\% \cdot p + 2\%$
-1.0 – 1.0	$\sigma_p/p \sim 0.04\% \cdot p + 1\%$
1.0 – 2.5	$\sigma_p/p \sim 0.04\% \cdot p + 2\%$
2.5 – 3.5	$\sigma_p/p \sim 0.2\% \cdot p + 5\%$
	EM Calorimeters
-3.5 – -2.0	$1\%/E + 2.5\%/\sqrt{E} + 1\%$
-2.0 – -1.0	$2\%/E + 8\%/\sqrt{E} + 2\%$
-1.0 – 1.0	$2\%/E + 14\%/\sqrt{E} + 3\%$
1.0 – 3.5	$2\%/E + 12\%/\sqrt{E} + 2\%$
	Far-Forward region: protons
	$\sigma_p/p = 5\%$ and $\sigma_{P_t}/P_t = 3\%$

7. Simulation of the double spectator tagging with FF detectors

The full simulation framework EicRoot was used to study the performance of detectors which are intended to be used in the FF region for detection of two spectator protons. 200k DIS events were generated with the CLASDIS. SRC and 3BBU-MF regimes were added separately and in total 400k events were processed with EicRoot. Information provided by the EicRoot was used to reconstruct momenta of two spectator protons. Events from the SRC and 3BBU-MF regimes were weighted with their respective strengths (Table 1) and finally combined to obtain the simulation of the spectator double tagging with FF detectors of the ^{3}He$(e, e' p_{s1} p_{s2})X$ channel. The sum of momenta of two spectator protons in the fixed target frame is approximately equal to the initial momentum of the struck neutron in ^{3}He, as presented in Fig. 5.

By constraining these spectator nucleons at small angle (along the ion beam direction) in the collider frame and their total momentum close to zero in fixed target frame, the DIS events from a "free" neutron with minimal off-shell effects can be selected. By tagging two low momentum protons after electron and polarized ^{3}He beam scattering, one can minimize nuclear corrections and gain unique access to:

- the asymmetry $A_1^{^3\text{He}}$ and A_1^n as a function of x_B;
- the neutron structure function $F_2^{^3\text{He}}$ and F_2^n as a function of x_B.

8. Inclusive DIS vs. inclusive DIS with double spectator tagging

Experimentally, the virtual photon asymmetry A_1 can be extracted from the measured longitudinal electron asymmetry $A_{||}$ and transverse electron asymmetry $A_\perp$ where

$$A_{||} = \frac{\sigma_{\downarrow\Uparrow} - \sigma_{\uparrow\Uparrow}}{\sigma_{\downarrow\Uparrow} + \sigma_{\uparrow\Uparrow}} \quad \text{and} \quad A_\perp = \frac{\sigma_{\downarrow\Rightarrow} - \sigma_{\uparrow\Rightarrow}}{\sigma_{\downarrow\Rightarrow} + \sigma_{\uparrow\Rightarrow}}.$$

Considering electromagnetic interaction only, $\sigma_{\downarrow\Uparrow}(\sigma_{\uparrow\Uparrow})$ is the cross section of the electron spin anti-parallel (parallel) to beam direction scatter off the longitudinally polarized target. $\sigma_{\downarrow\Rightarrow}(\sigma_{\uparrow\Rightarrow})$ is the cross section of the electron spin ani-parallel (parallel) scatter off the transversely polarized target. The relation between A_1, $A_{||}$ and $A_\perp$ is

$$A_1 = \frac{A_{||}}{D(1 + \eta\xi)} - \frac{\eta A_\perp}{d(1 + \eta\xi)}, \qquad (2)$$
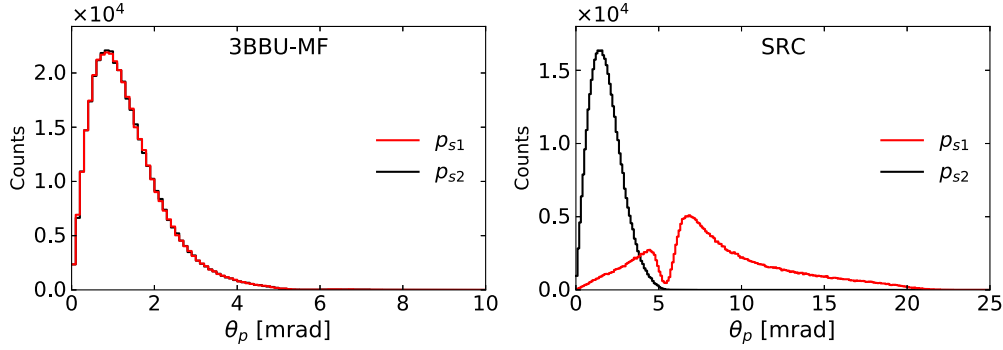
Fig. 4. Distribution of the scattering angle θ_p of both spectator protons in case of the 3BBU-MF and SRC nuclear effects. The gap in the angular distribution for the SRC case is due to gap in the detector acceptance in the far-forward region, as it is summarized in Table 2.
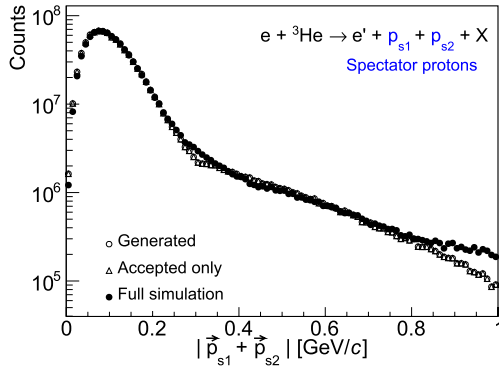
Fig. 5. Distribution of the vector sum of two spectator protons' momentum, p_{s1} and p_{s2}, in the fixed target frame for kinematic setting 5×41 GeV/n. The simulation is shown at the generated level, including acceptance correction, and including full simulation with smearing effects, using open circles, open triangles and the solid points, respectively. In general, for both 3BBU-MF and SRC protons included in this figure, the acceptance is $\sim$90% or better except in the gap regions between detector subsystems.

where $D = y(2-y)(2+\gamma^2 y)/(2(1+\gamma^2)y^2 + (4(1-y)-\gamma^2 y^2)(1+R))$, $d = \sqrt{4(1-y)-\gamma^2 y^2} D/(2-y)$, $\eta = \gamma(4(1-y)-\gamma^2 y^2)/(2-y)/(2+\gamma^2 y)$, $\xi = \gamma(2-y)/(2+\gamma^2 y)$, $\gamma = 4M^2 x^2/Q^2$ [38,14] and R is the ratio of the longitudinal and transverse virtual photon absorption cross sections σ_L/σ_T [39]. The world fit parameters in Ref. [40] are used to calculate value of R. However, the analysis within this work focuses only on A_1^n.

The procedure applied in extracting A_1^n from $A_1^{^3\text{He}}$ through inclusive (e, e') measurement and directly measured A_1^n using the double spectator tagging method is described in this section.

- The values of A_1^n and A_1^p are taken from the parameterization provided in [14]. The uncertainties and the correlation matrix associated with A_1^n and A_1^p parameterization have also been obtained from [14].
- The structure functions F_2^p and F_2^D are taken from the world data fit NMC E155 [41]. The larger of the asymmetric uncertainties is chosen as the symmetric uncertainty for these structure functions.
- Assuming no off-shell or nuclear-motion corrections, the value of F_2^n is obtained using $F_2^n = F_2^D - F_2^p$. Similarly, $F_2^{^3\text{He}}$ is obtained by using $F_2^{^3\text{He}} = F_2^D + F_2^p$. The uncertainties of F_2^n and $F_2^{^3\text{He}}$ are propagated from the uncertainties of F_2^D and F_2^p.
- The effective polarization of neutron and proton is $P_n = 0.86 \pm 0.02$ and $P_p = -0.028 \pm 0.004$ taken from [42]. Similarly, the polarization of the electron beam P_e and the polarization of the ion beam P_N are both $70 \pm 1\%$ as was stated in the EIC Yellow Report [35].

- The value of $A_1^{^3\text{He}}$ can be approximated by:

$$A_1^{^3\text{He}} = \underbrace{P_n \frac{F_2^n}{F_2^{^3\text{He}}} A_1^n}_{(1)} + \underbrace{2 P_p \frac{F_2^p}{F_2^{^3\text{He}}} A_1^p}_{(2)}, \tag{3}$$

where (1) and (2) are the neutron and the proton contributions to the asymmetry respectively. This is a simple composition model which shows how polarized $A_1^{^3\text{He}}$ can be described in terms of A_1^n. In reality, there are many other nuclear corrections which need to be included (ex. off-shell effects), increasing the model-dependent uncertainty.

- In order to have good statistics in selected x_B ranges, 400k of events were generated for each of three different x_B ranges: $0.0026 < x_B < 1$, $0.2 < x_B < 1$ and $0.5 < x_B < 1$. This was repeated for unpolarized neutrons and polarized neutrons with polarizations $+1$ and -1. This resulted in a total of 2.4 million generated events. These events were then used to separately add SRC and 3BBU-MF regimes. As such, 4.8 million events were processed by the Eic-smear framework. Therefore, fast simulation framework Eic-smear with FF detectors was used to process these data.

Our results are shown for integrated e-nucleon luminosity of 100 fb^{-1} which corresponds to 115 days of running at 100% efficiency with a e-nucleon luminosity of 10^{34} cm^{-2} s^{-1} [35]. We assume to measure longitudinal and transverse asymmetry with the same integrated luminosity. The total events thus pass all selection cuts were binned in x_B. In this analysis, the reconstructed x_B was calculated following the standard inclusive method in which only the reconstructed momentum information of the scattered electron was used.[3] Due to resolution effects and a rapidly decreasing cross section, this technique is limited to $x_B = 0.75$ for the proposed EIC detector [35]. Also, for a given reconstructed x_B bin, the average value of generated x_B (x-avg) was calculated and plotted at this value [44]. Similarly, the generated-average Q^2 (Q^2-avg) for a given x_B was calculated. The absolute uncertainty obtained is statistical and given by:

$$\delta A_{||,\perp}^{^3\text{He}(n)} = \frac{1}{\sqrt{N} P_e P_N}, \tag{4}$$

where N is the total number of events obtained after scaling the generated events to EIC luminosity. The $\delta A_1^{^3\text{He}(n)}$ is the propagation uncertainty of $\delta A_{||,\perp}^{^3\text{He}(n)}$ through Eq. (2). At the high value of Q^2, both variables η and ξ are close to zero

---

[3] For different methods to determine x_B and Q^2 see Ref. [43].
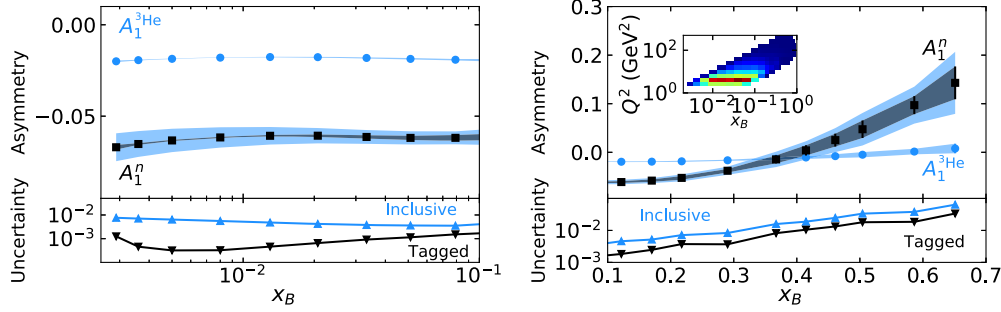
Fig. 6. A direct comparison of A_1^n extracted from inclusive measurements (blue band) and tagged measurements (black square) which are superimposed on the blue band. The left plot is for $x \le 0.1$ and the right plot is for $x \ge 0.1$. The blue points are the $A_1^{3\text{He}}$ measured values from inclusive measurements from which the blue band is extracted. The uncertainties for both the techniques are compared in the bottom box where the blue (black inverted) triangles are the absolute uncertainties of inclusive (tagged) measurements. The data points were located at the average value for each x_B bin. The asymmetry calculation for each data point corresponds to the average value of Q^2 for each x_B bin.

which makes the contribution of $\delta A_\perp^{3\text{He}(n)}$ to $\delta A_1^{3\text{He}(n)}$ small ($< 1\%$). Thus, for this measurement if the transverse integrated luminosity was only 10 fb^{-1} it would not significantly effect the results.

- Using the obtained value of $A_1^{3\text{He}}$ from the previous step, A_1^p from [14], F_2^p and F_2^D from fit NMC E155 [41], and $P_{p(n)}$ from [42], we extract A_1^n using Eq. (3). The total A_1^n uncertainty (shown as a blue band in Fig. 6) is propagated from the statistical uncertainty of $A_1^{3\text{He}}$, and systematic uncertainty from A_1^p, F_2^n, F_2^D and $P_{p(n)}$.

- Double tagged events are selected using DIS cuts and requiring a condition on these two spectator protons with additional cut on $|\vec{p}_{s1} + \vec{p}_{s2}| < 0.1$ GeV/c in the fixed target frame. The uncertainty of A_1^n from the double tagging simulation is statistical and calculated using Eq. (4). F_2^n can also be obtained directly using the same double spectator approach but we use the value obtained from $F_2^n = F_2^D - F_2^p$ in the extraction for simplicity.

- The A_1^n obtained from a traditional extraction using a fixed target as well as the one obtained directly from the double spectator tagging method are shown in Fig. 6. A comparison of the associated uncertainties using these two methods is shown in a box at the bottom of Fig. 6. For equal integrated luminosity, the tagged measurements provide a significant improvement on the statistical uncertainty as well as overall uncertainty from the extraction procedure, which is dominated by model dependent uncertainties from F_2^n, P_p and A_1^p for the fixed-target case.

The advantage of the double spectator tagging approach is that this method minimizes the uncertainty in the proton polarization, P_p which is typically model dependent and $\sim 10\%$. While there is a good overlap ($0.4 < x_B < 0.65$) with the A_1^n measurement conducted in Hall C at Jefferson Lab [45], this work provides a complementary measurement at much higher Q^2 values thereby expanding the available world data on A_1^n.

9. Radiative and electroweak corrections

The effects of electromagnetic radiation on this measurement were studied using the DJANGOH event generator [46,47], which includes full radiative cross section calculations for DIS events, including the emission of radiative photons distorting the measured (leptonic) values of x_B and Q^2 from those of the vertex (hadronic). Using the nuclear Parton Distribution Functions for ^{3}He from nCTEQ15 [48], an inclusive sample of DIS events from ^{3}He was generated and the effects of experimental acceptance and resolution was applied using Eic-smear. The simulated yields were
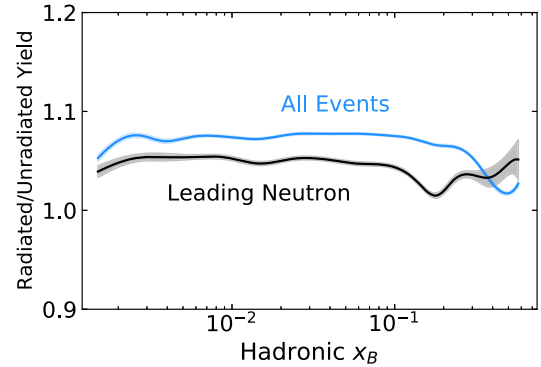
Fig. 7. The ratio between the simulated yield in hadronic x_B for the DJANGOH samples with and without radiative effects included. The ratio is shown both for the full sample of events and for the subset of events resulting from leading neutrons, though the effects of spectator acceptance were not included in these simulations.

compared for the case with radiative generation and the case with radiation disabled, for both the full event sample and the subset of events resulting from an initial-state neutron.

The primary effect of single-photon emission was found to be to lower the leptonic value of x_B from that of the interaction, as well as to smear the leptonic value of Q^2. This has an apparently large effect on the measured distributions, particularly inflating the yield in the lowest-x_B kinematic bins. However, the primary concern for measurements of A_1^n is the coverage in the hadronic kinematic variables. The effect of radiation on the coverage of hadronic x_B, shown in Fig. 7, was found to be significantly smaller, comprising a $< 10\%$ impact on yield over the measured bins and therefore a $< 5\%$ impact on statistical precision. This was found to be the case both for the full set of simulated DIS events and for those events which resulted from a leading neutron, indicating a similarly small effect for both the inclusive and tagged measurements.

In an analysis of this data, which would include such radiative effects, it would be necessary to compare with physics models such as DJANGOH which fully calculate the impact of radiation on the interaction, with the addition of the spectator system for fully tagged events. By including possible models for A_1 in the event generation and using realistic detector models, all physics and experimental effects can be convoluted into pseudodata for comparison with measured data, both for the inclusive and tagged case. This method avoids possible model-dependencies in the A_1^n extraction which would result from attempting to correct data for radiative effects and would allow inference on fit parameters for the model of A_1^n.

Finally, while the simulations in this work use pure electromagnetic structure functions, real data in these EIC kinematics

will have electroweak contributions to the asymmetry which must be considered. For elastic scattering, the electroweak (*i.e.* parity-violating) contribution to the asymmetry is as large as 10^{-4} [49], much smaller than the 1% asymmetry found herein for ^{3}He. Elastic scattering decreases with Q^2 much faster than DIS, which to first order is constant in Q^2; thus, the parity-violating contribution of electromagnetic DIS/SIDIS due to weak interactions is expected to be a significant correction for precise measurements only in certain kinematics, *e.g.* for large Q^2. Consideration of parity-violating asymmetries will require their calculation bin-by-bin in the kinematics of the experiment.

10. Conclusion

We have shown that with the advent of the EIC, neutron structure can be investigated through the unique far-forward detection capabilities to tag double spectator protons – remnants of electron scattering events from the neutron in polarized ^{3}He ions. This double spectator tagging technique greatly reduces the systematic uncertainties thereby allowing an extraction of A_1^n in a precise and model independent manner while simultaneously determining the validity of multiple theoretical models used in A_1^n extraction for fixed target scenarios. Improvement in precision in A_1^n as compared to inclusive extractions is found to be a factor of 3 over all kinematics and greater than an order-of-magnitude in the low-x_B region. This novel approach provides crucial new information to our understanding of the role of valence quarks in neutron spin structure with far less model dependence than other techniques, and will help to reveal possible quark orbital angular momentum contributions to the spin structure of the neutron.

Declaration of competing interest

The authors declare that they have no known competing financial interests or personal relationships that could have appeared to influence the work reported in this paper.

Acknowledgements

References

[1] S.E. Kuhn, J.P. Chen, E. Leader, Spin structure of the nucleon - status and recent results, Prog. Part. Nucl. Phys. 63 (2009) 1–50, https://doi.org/10.1016/j.ppnp. 2009.02.001, arXiv:0812.3535.

[2] E. Leader, C. Lorcé, The angular momentum controversy: what's it all about and does it matter?, Phys. Rep. 541 (3) (2014) 163–248, https://doi.org/10.1016/j. physrep.2014.02.010, arXiv:1309.4235.

[3] J. Ashman, European Muon Collaboration, A measurement of the spin asymmetry and determination of the structure function g₁ in deep inelastic muon-proton scattering, Phys. Lett. B 206 (2) (1988) 364–370, https://doi.org/10.1016/ 0370-2693(88)91523-7.

[4] C.A. Aidala, S.D. Bass, D. Hasch, G.K. Mallot, The spin structure of the nucleon, Rev. Mod. Phys. 85 (2013) 655–691, https://doi.org/10.1103/RevModPhys. 85.655, https://link.aps.org/doi/10.1103/RevModPhys.85.655.

[5] X. Ji, F. Yuan, Y. Zhao, What we know and what we don't know about the proton spin after 30 years, Nat. Rev. Phys. 3 (1) (2021) 27–38, https://doi.org/ 10.1038/s42254-020-00248-4, arXiv:2009.01291.

[6] X. Zheng, et al., Precision measurement of the neutron spin asymmetry A1**N and spin flavor decomposition in the valence quark region, Phys. Rev. Lett. 92 (2004) 012004, https://doi.org/10.1103/PhysRevLett.92.012004, arXiv:nucl-ex/0308011.

[7] A. Freese, I.C. Cloët, Quark spin and orbital angular momentum from proton generalized parton distributions, Phys. Rev. C 103 (4) (2021) 045204, https:// doi.org/10.1103/PhysRevC.103.045204, arXiv:2005.10286.

[8] A. Deur, S.J. Brodsky, G.F. De Téramond, The spin structure of the nucleon, Rep. Prog. Phys. 82 (2019) 076201, https://doi.org/10.1088/1361-6633/ab0b8f, arXiv: 1807.05250.

[9] D. Akimov, et al., The COHERENT experiment at the spallation neutron source, arXiv:1509.08702, 2015.

[10] A. Bodek, et al., Experimental studies of the neutron and proton electromagnetic structure functions, Phys. Rev. D 20 (1979) 1471–1552, https://doi.org/10. 1103/PhysRevD.20.1471.

[11] J. Arrington, F. Coester, R.J. Holt, T.S.H. Lee, Neutron structure functions, J. Phys. G 36 (2009) 025005, https://doi.org/10.1088/0954-3899/36/2/025005, arXiv: 0805.3116.

[12] P.L. Anthony, et al., Determination of the neutron spin structure function, Phys. Rev. Lett. 71 (1993) 959–962, https://doi.org/10.1103/PhysRevLett.71.959.

[13] V. Sulkosky, et al., Measurement of the ^{3}He spin-structure functions and of neutron (^{3}He) spin-dependent sum rules at $0.035 \leq Q^2 \leq 0.24$ GeV^2, Phys. Lett. B 805 (2020) 135428, https://doi.org/10.1016/j.physletb.2020.135428, arXiv:1908.05709.

[14] X. Zheng, et al., Precision measurement of the neutron spin asymmetries and spin-dependent structure functions in the valence quark region, Phys. Rev. C 70 (2004) 065207, https://doi.org/10.1103/PhysRevC.70.065207, arXiv:nucl-ex/ 0405006.

[15] J. Adam, et al., Electron ion collider conceptual design report, https://www.bnl. gov/ec/files/EIC_CDR_Final.pdf, 2021.

[16] J. Maxwell, C. Epstein, R. Milner, J. Alessi, E. Beebe, A. Pikin, J. Ritter, A. Zelenski, Development of a polarized helium-3 source for RHIC and eRHIC, Int. J. Mod. Phys. Conf. Ser. 40 (01) (2016) 1660102, https://doi.org/10.1142/ S2010194516601022.

[17] N. Baillie, et al., Measurement of the neutron F2 structure function via spectator tagging with CLAS, Phys. Rev. Lett. 108 (2012) 142001, https://doi.org/10. 1103/PhysRevLett.108.142001, arXiv:1110.2770, Erratum: Phys. Rev. Lett. 108 (2012) 199902.

[18] S. Tkachenko, et al., Measurement of the structure function of the nearly free neutron using spectator tagging in inelastic ^{2}H(e, e'p)X scattering with CLAS, Phys. Rev. C 89 (2014) 045206, https://doi.org/10.1103/PhysRevC.89.045206, arXiv:1402.2477, Addendum: Phys. Rev. C 90 (2014) 059901.

[19] W. Cosyn, V. Guzey, D.W. Higinbotham, C. Hyde, S. Kuhn, P. Nadel-Turonski, K. Park, M. Sargsian, M. Strikman, C. Weiss, Neutron spin structure with polarized deuterons and spectator proton tagging at EIC, J. Phys. Conf. Ser. 543 (2014) 012007, https://doi.org/10.1088/1742-6596/543/1/012007, arXiv:1409.5768.

[20] W. Cosyn, C. Weiss, Neutron spin structure from polarized deuteron DIS with proton tagging, Phys. Lett. B 799 (2019) 135035, https://doi.org/10.1016/j. physletb.2019.135035, arXiv:1906.11119.

[21] W. Cosyn, C. Weiss, Polarized electron-deuteron deep-inelastic scattering with spectator nucleon tagging, Phys. Rev. C 102 (2020) 065204, https://doi.org/10. 1103/PhysRevC.102.065204, arXiv:2006.03033.

[22] D. Flay, et al., Measurements of d_2^n and A_1^n: probing the neutron spin structure, Phys. Rev. D 94 (5) (2016) 052003, https://doi.org/10.1103/PhysRevD.94. 052003, arXiv:1603.03612.

[23] M. Mihovilovič, et al., Measurement of double-polarization asymmetries in the quasi-elastic $^3\vec{\text{He}}(\vec{e}, e'p)$ process, Phys. Lett. B 788 (2019) 117–121, https://doi. org/10.1016/j.physletb.2018.10.063, arXiv:1804.06043.

[24] M. Mihovilovic, et al., Measurement of double-polarization asymmetries in the quasielastic $^3\vec{\text{He}}(\vec{e}, e'd)$ process, Phys. Rev. Lett. 113 (23) (2014) 232505, https://doi.org/10.1103/PhysRevLett.113.232505, arXiv:1409.2253.

[25] E. Long, et al., Measurement of the single-spin asymmetry A_y^0 in quasi-elastic $^3\text{He}^\uparrow(e, e'n)$ scattering at $0.4 < Q^2 < 1.0$ GeV/c^2, Phys. Lett. B 797 (2019) 134875, https://doi.org/10.1016/j.physletb.2019.134875, arXiv:1906.04075.

[26] R. Cruz-Torres, et al., Probing few-body nuclear dynamics via ^{3}H and ^{3}He (e, e'p)pn cross-section measurements, Phys. Rev. Lett. 124 (21) (2020) 212501, https://doi.org/10.1103/PhysRevLett.124.212501, arXiv:2001.07230.

[27] P.L. Anthony, et al., Measurements of the Q**2 dependence of the proton and neutron spin structure functions g(1)**p and g(1)**n, Phys. Lett. B 493 (2000) 19–28, https://doi.org/10.1016/S0370-2693(00)01014-5, arXiv:hep-ph/0007248.

[28] J.I. Friedman, H.W. Kendall, Deep inelastic electron scattering, Annu. Rev. Nucl. Part. Sci. 22 (1972) 203–254, https://doi.org/10.1146/annurev.ns.22.120172. 001223.

[29] L. Mankiewicz, A. Schafer, M. Veltri, PEPSI: a Monte Carlo generator for polarized leptoproduction, Comput. Phys. Commun. 71 (1992) 305–318, https://doi.org/10.1016/0010-4655(92)90016-R.

[30] C. Ciofi degli Atti, L. Kaptari, On the interpretation of the processes He-3(e,e-prime p) H-2 and He-3(e,e-prime p) (pn) at high missing momenta, Phys. Rev. Lett. 95 (2005) 052502, https://doi.org/10.1103/PhysRevLett.95.052502, arXiv:nucl-th/0502045.

[31] J. Pybus, I. Korover, R. Weiss, A. Schmidt, N. Barnea, D. Higinbotham, E. Piasetzky, M. Strikman, L. Weinstein, O. Hen, Generalized contact formalism analysis of the ^{4}He$(e, e'pN)$ reaction, Phys. Lett. B 805 (2020) 135429, https://doi.org/10.1016/j.physletb.2020.135429, arXiv:2003.02318.

[32] R. Cruz-Torres, D. Lonardoni, R. Weiss, N. Barnea, D. Higinbotham, E. Piasetzky, A. Schmidt, L. Weinstein, R. Wiringa, O. Hen, Scale and scheme independence and position-momentum equivalence of nuclear short-range correlations, Nat. Phys. (2020), https://doi.org/10.1038/s41567-020-01053-7.

[33] L. Frankfurt, M. Strikman, High-energy phenomena, short range nuclear structure and QCD, Phys. Rep. 76 (1981) 215–347, https://doi.org/10.1016/0370-1573(81)90129-0.

[34] S. Agostinelli, et al., GEANT4—a simulation toolkit, Nucl. Instrum. Methods A 506 (2003) 250, https://doi.org/10.1016/S0168-9002(03)01368-8.

[35] R. Abdul Khalek, et al., Science Requirements and Detector Concepts for the Electron-Ion Collider, EIC Yellow Report, 2021, arXiv:2103.05419.

[36] Z. Tu, A. Jentsch, M. Baker, L. Zheng, J.H. Lee, R. Venugopalan, O. Hen, D. Higinbotham, E.C. Aschenauer, T. Ullrich, Probing short-range correlations in the deuteron via incoherent diffractive J/Psi production with spectator tagging at the EIC, Phys. Lett. B 811 (2020) 135877, https://doi.org/10.1016/j.physletb.2020.135877.

[37] https://eic.github.io/software/eicsmear.html#matrix-02, 2021.

[38] N. Sato, W. Melnitchouk, S.E. Kuhn, J.J. Ethier, A. Accardi, Iterative Monte Carlo analysis of spin-dependent parton distributions, Phys. Rev. D 93 (7) (2016) 074005, https://doi.org/10.1103/PhysRevD.93.074005, arXiv:1601.07782.

[39] R.P. Feynman, Photon-Hadron Interactions, 1973.

[40] K. Abe, et al., Measurements of $R = \sigma(L)/\sigma(T)$ for $0.03 < x < 0.1$ and fit to world data, Phys. Lett. B 452 (1999) 194–200, https://doi.org/10.1016/S0370-2693(99)00244-0, arXiv:hep-ex/9808028.

[41] M. Arneodo, et al., Measurement of the proton and the deuteron structure functions, F2(p) and F2(d), Phys. Lett. B 364 (1995) 107–115, https://doi.org/10.1016/0370-2693(95)01318-9, arXiv:hep-ph/9509406.

[42] F.R.P. Bissey, V.A. Guzey, M. Strikman, A.W. Thomas, Complete analysis of spin structure function g(1) of He-3, Phys. Rev. C 65 (2002) 064317, https://doi.org/10.1103/PhysRevC.65.064317, arXiv:hep-ph/0109069.

[43] J. Blumlein, The theory of deeply inelastic scattering, Prog. Part. Nucl. Phys. 69 (2013) 28–84, https://doi.org/10.1016/j.ppnp.2012.09.006, arXiv:1208.6087.

[44] G.D. Lafferty, T.R. Wyatt, Where to stick your data points: the treatment of measurements within wide bins, Nucl. Instrum. Methods A 355 (1995) 541–547, https://doi.org/10.1016/0168-9002(94)01112-5.

[45] X. Zheng, G. Cates, J. Chen, Z. Meziani, Measurement of neutron spin asymmetry A_1^n in the valence quark region using an 11 GeV beam and a Polarized ^{3}He target in Hall C, proposal E12-06-110, 2006.

[46] A. Kwiatkowski, H. Spiesberger, H.J. Mohring, Heracles: an event generator for ep interactions at HERA energies including radiative processes: version 1.0, Comput. Phys. Commun. 69 (1992) 155–172, https://doi.org/10.1016/0010-4655(92)90136-M.

[47] K. Charchula, G.A. Schuler, H. Spiesberger, Combined QED and QCD radiative effects in deep inelastic lepton - proton scattering: the Monte Carlo generator DJANGO6, Comput. Phys. Commun. 81 (1994) 381–402, https://doi.org/10.1016/0010-4655(94)90086-8.

[48] K. Kovarik, et al., nCTEQ15 - global analysis of nuclear parton distributions with uncertainties in the CTEQ framework, Phys. Rev. D 93 (8) (2016) 085037, https://doi.org/10.1103/PhysRevD.93.085037, arXiv:1509.00792.

[49] C. Sofiatti, T.W. Donnelly, Polarized e-p elastic scattering in the collider frame, Phys. Rev. C 84 (2011) 014606, https://doi.org/10.1103/PhysRevC.84.014606, arXiv:1104.2149.